JCTC Journal of Chemical Theory and Computation

Article

pubs.acs.org/JCTC

Polarizabilities of π-Conjugated Chains Revisited: Improved Results from Broken-Symmetry Range-Separated DFT and New CCSD(T) Benchmarks

M. Belén Oviedo, Niranjan V. Ilawe, and Bryan M. Wong*

Department of Chemical & Environmental Engineering and Materials Science & Engineering Program, University of California-Riverside, Riverside, California 92521,United States

Supporting Information

ABSTRACT: We present a detailed analysis of nonempirically tuned range-separated functionals, with both short- and long-range exchange, for calculating the static linear polarizability and second hyperpolarizabilities of various polydiacetylene (PDA) and polybutatriene (PBT) oligomers. Contrary to previous work on these systems, we find that the inclusion of some amount of short-range exchange does improve the accuracy of the computed polarizabilities and second hyperpolarizabilities. Most importantly, in contrast to prior studies on these oligomers, we find that the lowest-energy electronic states for PBT are *not* closed-shell singlets, and enhanced accuracy with range-separated DFT can be obtained by allowing the system to relax to a lower-energy broken-symmetry solution. Both the computed polarizabilities and second hyperpolarizabilities for PBT are significantly improved with these broken-symmetry solutions when compared to previously published and current benchmarks. In addition to these new analyses, we provide new large-scale CCSD(T) and explicitly correlated CCSD(T)-F12 benchmarks for the PDA and PBT systems, which comprise the most complete and accurate calculations of linear polarizabilities and second hyperpolarizabilities on these systems to date. These new CCSD(T) and CCSD(T)-F12 benchmarks confirm our DFT results and emphasize the importance of broken-symmetry effects when calculating polarizabilities and hyperpolarizabilties of π-conjugated chains.

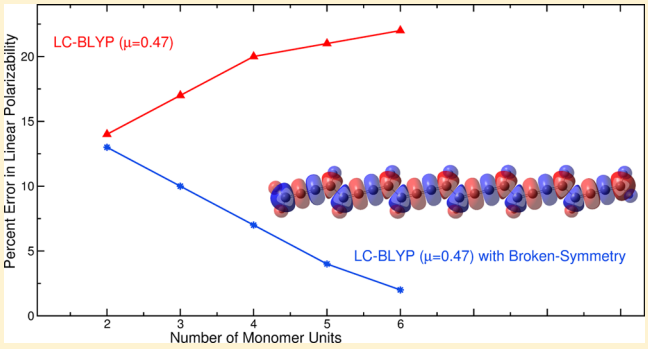

INTRODUCTION

Since the early 1960s,[1−3] the linear and nonlinear optical (NLO) properties of π-conjugated polymers have garnered immense interest from both theorists[4,5] and experimentalists[6,7] for their use as novel optical materials. Specifically, recent developments in these NLO materials have led to a wide variety of technological advancements including optical memory, holography, optical computing, nonlinear microscopy, and electro-optic waveguide devices.[8] Predictive computational design, particularly with quantum chemical methods, will play an important role in these advancements by providing a rational and guided path for accurately calculating the NLO properties in these conjugated materials. Among the various quantum chemical techniques currently in use, the most accurate calculations of polarizabilities and second hyperpolarizabilities of polymers have been obtained with wave function-based techniques (such as coupled cluster methods); however, these calculations have been limited to short polyenes due to their high computational costs.[9] In contrast, the simple Hartree−Fock method is sometimes still employed for the calculation of hyperpolarizabilities of large molecules; unfortunately, the Hartree−Fock formalism by definition does not fully account for dynamic electron correlation, which plays an important role in the estimation of polarizabilities and hyperpolarizabilities (see refs 10 and 11 and references therein). Kohn−Sham density functional theory (DFT), which includes an approximate treatment of electron correlation, has become an extremely popular and versatile method for its excellent balance between accuracy and computational cost;[12] nevertheless, the selection of appropriate exchange-correlation (XC) functionals for calculating polarizabilities and hyperpolarizabilities still remains.

Historically, the accurate calculation of polarizabilites in π-conjugated systems has presented an immense challenge for conventional DFT methods. In particular, previous work by others[4,5,13−15] has demonstrated that DFT calculations with common XC-functionals, including LDA, GGA, and functionals constructed with a fixed percentage of exact exchange, dramatically fail to provide an accurate description of both the linear polarizability (α) and the second hyperpolarizability (γ) of one-dimensional polymers. These difficulties stem from the fact that polarizabilities are second-order electronic properties and, as mentioned previously, will be extremely

Received: April 9, 2016
Published: June 22, 2016

DOI: 10.1021/acs.jctc.6b00360
J. Chem. Theory Comput. 2016, 12, 3593−3602

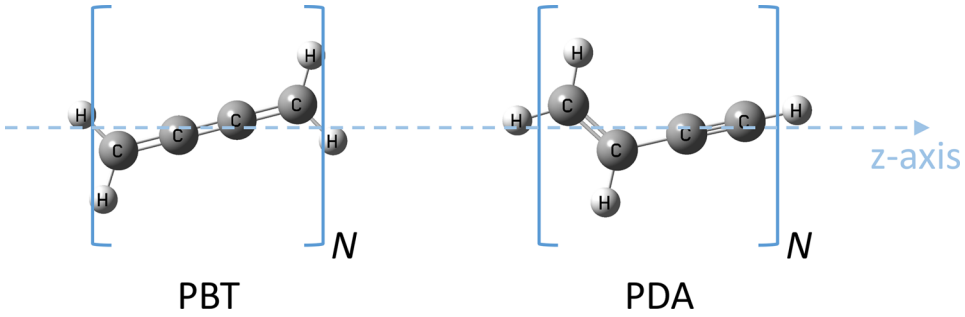

Figure 1. Molecular structures of the PBT and PDA oligomers (N = 1−6) studied in this work. The longitudinal linear polarizability and second hyperpolarizability of both structures are computed along the z-axis shown in the figure.

sensitive to exchange-correlation approximations in Kohn−Sham DFT methods (in particular, for computing γ). In a very recent paper by Champagne and co-workers,[16] the authors employed both standard and nonempirically tuned range-separated functionals (specifically CAM-B3LYP and LC-BLYP) to calculate the longitudinal linear polarizability and second hyperpolarizability of polydiacetylene (PDA) and polybutatriene (PBT) oligomers (Figure 1). To test the accuracy of these various range-separated methods, the authors utilized a limited set of coupled-cluster methods with single and double excitations and perturbative triple excitations, CCSD(T), in conjunction with second-order and fourth-order Møller−Plesset perturbation theory (MP2 and MP4) as benchmark standards. On the basis of these benchmarks, the authors concluded with the following statements: (1) "It is not expected that [adjusting the fraction of short-range HF exchange] will improve the polarizability and the second polarizability," (2) "For all levels of approximation, the overestimation of the α values [was observed]," and (3) "The bad performance of all levels of approximation to estimate γ of PBT chains [was observed]."

To shed additional light on these previous conclusions, we present a new, detailed investigation using (1) nonempirically tuned range-separated functionals that include a portion of short-range HF exchange and (2) an extensive analysis of broken-symmetry effects in range-separated functionals for calculating polarizabilities and second hyperpolarizabilies in PDA and PBT chains. In regard to the first point, previous work by our group[17] and others[18−21] has suggested that the inclusion of some short-range HF exchange *does* improve the accuracy of computed excited-state properties, and we demonstrate that this also enhances the accuracy of computed polarizabilities. Addressing the second point, broken-symmetry effects arise when the restricted (closed-shell) wave function becomes unstable toward an unrestricted (open-shell) solution.[22,23] In particular, we find that the lowest-energy electronic states for PBT are *not* closed-shell singlets, and enhanced accuracy with range-separated DFT can be obtained by allowing the system to relax to a lower-energy broken-symmetry solution. To both supplement and verify our findings, we also provide new large-scale CCSD(T) and explicitly correlated CCSD(T)-F12 benchmarks for the PDA and PBT systems. It is worth mentioning that in the original work by Champagne and co-workers,[16] only a limited set of CCSD(T) benchmark calculations were carried out due to the immense computational cost of these wave function-based methods (i.e., the largest PDA and PBT chains with five and six oligomers were not computed). For this reason, the authors commented that their range-separated calculations could not be checked to assess if the extrapolated DFT trends would either degrade or improve as a function of oligomer size. In this work, we complete these computationally intense CCSD(T) calculations as well as provide a new set of explicitly correlated CCSD(T)-F12 benchmarks which comprise the most complete and accurate calculations of polarizabilities and second hyperpolarizabilities on these systems to date. Taken together, our new broken-symmetry range-separated DFT calculations in conjunction with these high-level CCSD(T) and CCSD(T)-F12 benchmarks highlight the importance of broken-symmetry effects when calculating polarizabilities and hyperpolarizabilties of π-conjugated chains. Finally, we give a detailed analysis for all of these effects on various PDA and PBT oligomers and discuss the implications of both short-range exchange and broken-symmetry effects in calculating polarizabilities in these challenging systems.

Theory and Methodology. Since one of the main purposes of this work is to assess the accuracy of various range-separated functionals for computing polarizabilities, we briefly review the underlying theory for these methods. In contrast to conventional hybrid functionals, the range-separated formalism[24,25] mixes short-range density functional exchange with long-range Hartree−Fock exchange by partitioning the electron repulsion operator into short and long-range terms (i.e., the mixing parameter is a function of electron coordinates). In the most general form of the range-separated approach, the interelectronic Coulomb operator is given by[26,27]

$$\frac{1}{r_{12}} = \frac{1 - [\alpha + \beta\cdot\mathrm{erf}(\mu\cdot r_{12})]}{r_{12}} + \frac{[\alpha + \beta\cdot\mathrm{erf}(\mu\cdot r_{12})]}{r_{12}} \quad (1)$$

The erf term denotes the standard error function, r_{12} is the interelectronic distance between electrons 1 and 2, and μ is the range-separation parameter in units of Bohr^{-1}. The parameters, α and β, satisfy the following relations: $0 \le \alpha + \beta \le 1$, $0 \le \alpha \le 1$, and $0 \le \beta \le 1$. The parameter α in the partitioning allows a contribution of HF exchange over the entire range by a factor of α, and the parameter β allows us to incorporate long-range asymptotic HF exchange by a factor of $(\alpha + \beta)$. For example, the CAM-B3LYP functional of Yanai and co-workers[28] uses α = 0.19, $\alpha + \beta$ = 0.65, and μ = 0.33; however, the CAM-B3LYP functional *does not* incorporate a "full" range separation as it only has 65% HF exchange at long-range (instead of the correct 100% asymptotic HF exchange). In our previous work on range-separated functionals,[29−33] we have used and parametrized "full" range-separation schemes that correspond to setting α = 0.0 and β = 1.0. In particular, we[31] and others[34,35] have previously shown that maintaining a full 100% contribution of asymptotic HF exchange is essential for

DOI: 10.1021/acs.jctc.6b00360
J. Chem. Theory Comput. 2016, 12, 3593−3602

accurately describing valence excitations in even relatively simple molecular systems. For the two range-separated LC-BLYP methods used in this work, we fix $\alpha + \beta = 1.0$ (with different values of α) in conjunction with self-consistently tuning the range-separation parameter μ by satisfying DFT-Koopmans' theorem.[36−38] In summary, this theorem states that the energy of the highest occupied molecular orbital (HOMO) equals the negative of the ionization potential (IP), which is defined as the (ΔSCF) difference between the ground-state energy of the N electron and the $N - 1$ electron systems. Within the Kohn−Sham DFT formalism, this condition is fulfilled for the exact XC-functional; therefore, adjusting the range-separation parameter in this self-consistent manner provides a theoretical justification for this procedure. Although several numerical schemes exist, one practical approach for self-consistently tuning the range-separation parameter μ is to numerically minimize the following function:

$$J^2(\mu) = [\varepsilon^{\mu}_{\mathrm{HOMO}}(N) + \mathrm{IP}^{\mu}(N)]^2 + [\varepsilon^{\mu}_{\mathrm{HOMO}}(N+1) + \mathrm{IP}^{\mu}(N+1)]^2 \quad (2)$$

where $\varepsilon^{\mu}_{\mathrm{HOMO}}(N)$ is the HOMO energy of the N-electron system, and $\mathrm{IP}^{\mu}(N)$ is the ground-state energy difference between the N and $N - 1$ electron systems with the same range-separation parameter. The second term in this equation takes into account the $N + 1$ system to indirectly tune the LUMO energy of the N electron system. The LUMO energy cannot be directly incorporated in this equation since DFT−Koopmans' theorem does not explicitly relate the electron affinity (EA) to the negative of the LUMO energy.

To obtain the optimal μ values for each oligomer, several single-point energy calculations on fixed geometries (discussed further below) were carried out by varying μ from 0.0 to 0.4 (in increments of 0.02) for each of the N, $N + 1$, and $N - 1$ electron states. These calculations were computed using two nonempirically tuned LC-BLYP methods: The first method does not include any short-range exchange (i.e., $\alpha = 0.0$, $\beta = 1.0$), and the second method contains 20% exchange over the entire range (i.e., $\alpha = 0.2$, $\beta = 0.8$). It is important to emphasize that each of the different LC-BLYP parametrizations used in this work still recover the full 100% exchange at asymptotic distance ($\alpha + \beta = 1.0$) even though each parametrization has a different exchange contribution at short range. In addition, we also tested the performance of the LC-BLYP($\mu = 0.47$) method since there has been recent work demonstrating that hyperpolarizabilities of various chromophores are more accurately described without utilizing the nonempirically tuned procedure.[39] For all of the oligomers, we carried out a DFT stability analysis at all LC-BLYP levels of theory to converge (if possible) toward a lower-energy broken-symmetry solution, which allows for an unrestricted spin state as well as a reduction in symmetry of the orbitals. With the broken-symmetry solutions in hand, J^2 was computed (eq 2) as a function of μ for each polyene and all of the various monomers. Spline interpolation was subsequently used to refine the minimum for each individual system. All DFT calculations were carried out with the Gaussian 09 package[40] using default SCF convergence criteria (density matrix converged to at least 10^{-8}) and the default DFT integration grid (75 radial and 302 angular quadrature points).

In order to maintain a consistent comparison with the previous study of Champagne and co-workers, identical molecular geometries obtained from ref 16 were used throughout this work, and the Cartesian coordinates for all the systems are listed in the Supporting Information for completeness. Similarly, we utilized the same 6-31+G(d) basis set to compute the longitudinal static polarizability and second hyperpolarizability of the various PDA and PBT chains, ranging from one to six monomer units. Following the same approach by Champagne et al., all of the polarizabilities obtained with all DFT methods were calculated using analytical derivatives of the energy with respect to field strength within the coupled-perturbed Kohn−Sham (CPKS) method. Second hyperpolarizabilities for all DFT methods were evaluated as second-order numerical derivatives of the polarizability with respect to the applied external electric field. At the wave function-based CCSD(T) and explicitly correlated CCSD(T)-F12 levels of theory, polarizabilities and hyperpolarizabilities were manually calculated with a custom-developed code as the second- or fourth-order numerical derivatives of the energy with respect to the applied external electric field. In these finite field approaches, the following field amplitudes in atomic units (1 au = 5.142206×10^{11} V/m) were chosen: $F = 0.0, \pm 1 \times 10^{-4}, \pm 2 \times 10^{-4}, \pm 4 \times 10^{-4}, \pm 8 \times 10^{-4}, \pm 16 \times 10^{-4}$, and $\pm 32 \times 10^{-4}$ au. To maintain a consistent comparison with the various DFT methods, the CCSD(T) calculations were also performed with the same 6-31+G(d) basis set. In addition to the CCSD(T)/6-31+G(d) calculations, new CCSD(T)-F12 calculations were also carried out to verify both the overall trends and quality of the CCSD(T) benchmarks. The CCSD(T)-F12 methods have attracted recent attention for their ability to calculate extremely accurate electronic energies (typically at a higher level of accuracy than conventional CCSD(T) with the same basis) by constructing a wave function that depends explicitly on the interelectronic coordinates. As such, the explicitly correlated CCSD(T)-F12 methods exhibit dramatic improvements in basis set convergence, and results of quintuple-zeta quality that were obtained with smaller triple-ζ basis sets have previously been shown.[41] To this end, we carried out our CCSD(T)-F12 calculations with the cc-pVDZ basis, which is the largest basis set available that is commensurate with both the density-fitting algorithm in Molpro and our computational resources. As a side note, both the CCSD(T) and CCSD(T)-F12 calculations were extremely computationally intensive, especially for the large PDA[5], PDA[6], PBT[5], and PBT[6] structures. For example, the largest of these structures, PDA[6], took up to 18 continuous days (for *each* of the finite field F amplitudes) on 16 × 2.3 GHz AMD Opteron CPUs, and each calculation consumed up to 356 GB of disk space on rapid-access solid state drive storage. Finally, all of the CCSD(T)-F12 polarizabilities and second hyperpolarizabilites reported in this work were obtained from self-consistent CCSD(T)-F12a energies. The CCSD(T)-F12a energies were chosen over the CCSD(T)-F12b results since extensive benchmarks have shown that the CCSD(T)-F12a method gives better results for smaller basis sets (such as the cc-pVDZ basis set used in this work) than CCSD(T)-F12b.[42] The F12b variant differs from the F12a method by the inclusion of an additional energy correction which approximately doubles the magnitude of the coupling between the conventional and explicitly correlated pieces of the calculation.[42,43] Taken together, the CCSD(T)-F12 polarizabilities and second hyperpolarizabilities offer a second check on both the DFT and CCSD(T) results as well as provide new, additional high-quality benchmarks for the PDA and PBT systems.

DOI: 10.1021/acs.jctc.6b00360
J. Chem. Theory Comput. 2016, 12, 3593−3602

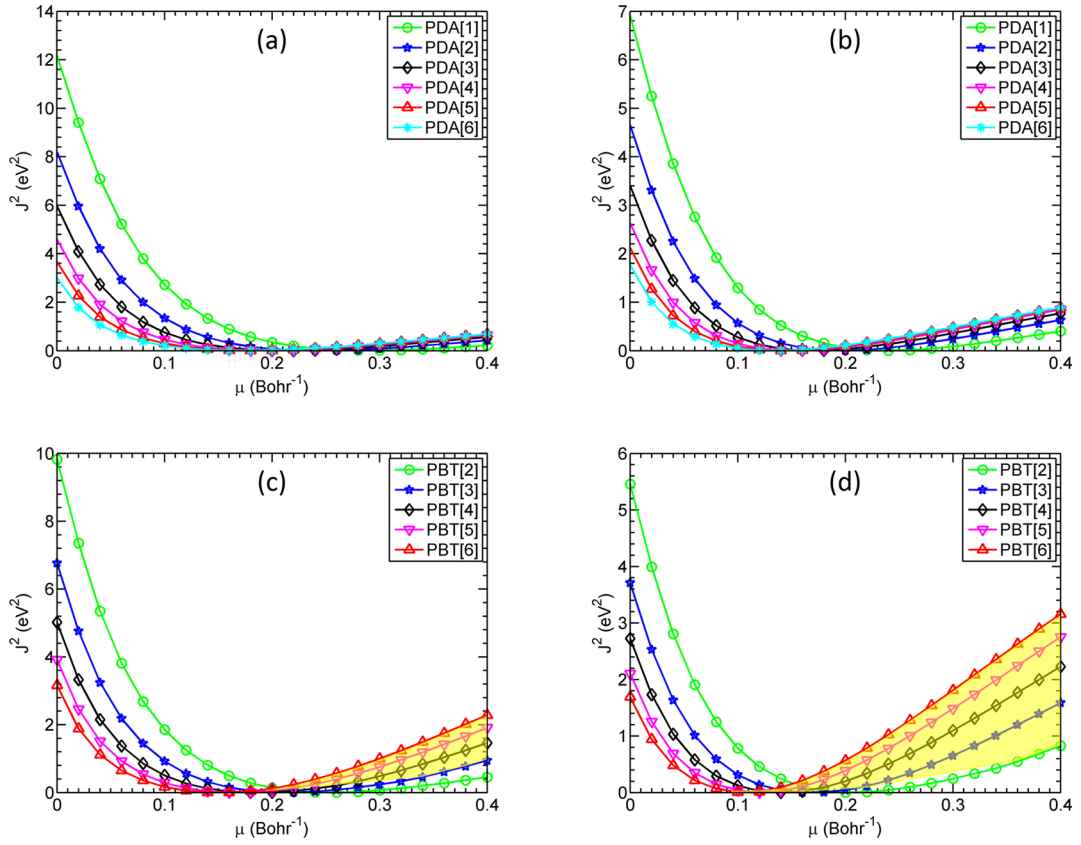

Figure 2. Plots of J^2 as a function of mu for (a) PDA without short-range exchange (LC-BLYP$_{\alpha=0.0,\beta=1.0}$), (b) PDA including short-range exchange (LC-BLYP$_{\alpha=0.2,\beta=0.8}$), (c) PBT without short-range exchange (LC-BLYP$_{\alpha=0.0,\beta=1.0}$), and (d) PBT including short-range exchange (LC-BLYP$_{\alpha=0.2,\beta=0.8}$). The shaded regions in (c) and (d) denote the values of μ where a symmetry-broken solution is obtained.

RESULTS AND DISCUSSION

Figure 2 shows the smooth curves that result from computing J^2 as a function of μ for (a) PDA without short-range exchange (LC-BLYP$_{\alpha=0.0,\beta=1.0}$), (b) PDA including short-range exchange (LC-BLYP$_{\alpha=0.2,\beta=0.8}$), (c) PBT without short-range exchange (LC-BLYP$_{\alpha=0.0,\beta=1.0}$), and (d) PBT including short-range exchange (LC-BLYP$_{\alpha=0.2,\beta=0.8}$). As discussed in the Theory and Methodology Section, we carried out a full DFT stability analysis at *all* LC-BLYP levels of theory for both PDA and PBT to allow (if possible) for a lower-energy broken-symmetry solution. As shown in Figure 2, only closed-shell solutions were obtained for PDA (regardless of μ value), whereas a broken-symmetry configuration was obtained for large values of μ in PBT for both LC-BLYP$_{\alpha=0.0,\beta=1.0}$ and LC-BLYP$_{\alpha=0.2,\beta=0.8}$. These results can be rationalized from the chemical structures of these systems since PDA is composed of successive double-single-triple-single CC bonds (cf. Figure 1) and is more alternant than PBT, which exhibits a single−double−double−double bond CC bond pattern (i.e., the π orbitals are much more strongly conjugated along the backbone of PBT compared to PDA). From a more theoretical viewpoint, range-separated functionals with higher values of μ inherently contain larger contributions of HF exchange in the XC potential, and it is well known[44−48] that DFT methods containing a large percentage of HF exchange will favor a lower-energy broken-symmetry configuration.[44−48] It is interesting to note that for sufficiently large values of μ, *all* PBT oligomers (even the smallest PBT[2] structure) will exhibit a broken-symmetry solution where the alpha and beta spin densities alternate through the whole backbone of the molecule, and a long-range ordering of the spin density persists as the length of the oligomer increases. This phenomenon corresponds to electrons localizing in the *p* orbitals of the carbon atoms in an antiferromagnetic pattern, which can be visualized as the spin density differences in Figure 3. Note that we *do not* obtain an antiferromagnetic pattern for PDA since the ground states for all of the PDA structures (regardless of μ) are closed-shell singlets, and the alpha and beta spatial distributions are the same.

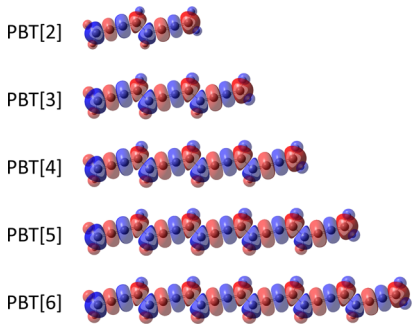

Figure 3. Spin density difference (blue = positive spin density and red = negative spin density) obtained with LC-BLYP(μ = 0.47) for the various PBT oligomers.

The optimally tuned μ values for PDA and PBT as obtained by both the LC-BLYP$_{\alpha=0.0,\beta=1.0}$ and LC-BLYP$_{\alpha=0.2,\beta=0.8}$ functionals are summarized in Table 1. It is interesting to note that the optimal μ values for both PDA and PBT are not affected by

DOI: 10.1021/acs.jctc.6b00360
J. Chem. Theory Comput. 2016, 12, 3593−3602

Table 1. Nonempirically Tuned μ Values for All Oligomers of PDA and PBT at the LC-BLYP/6-31+G(d) Level of Theory[a]

	PDA		PBT	
N	LC-BLYP (α = 0.0, β = 1.0)	LC-BLYP (α = 0.2, β = 0.8)	LC-BLYP (α = 0.0, β = 1.0)	LC-BLYP (α = 0.2, β = 0.8)
1	0.289 (0.294)	0.240		
2	0.241 (0.246)	0.196	0.254 (0.260)	0.205
3	0.212 (0.216)	0.170	0.213 (0.214)	0.168
4	0.194 (0.194)	0.153	0.185 (0.183)	0.142
5	0.181 (0.178)	0.142	0.166 (0.160)	0.125
6	0.172 (0.166)	0.134	0.151 (0.145)	0.111

[a]Numbers in parentheses are μ values obtained by Champagne et al.[16]

Table 2. Longitudinal Linear Polarizability and Second Hyperpolarizability for Increasingly Large PDA Oligomers at Various Levels of Theory[a]

N	CAM-B3LYP	CAM-B3LYP (BS)	LC-BLYP (α = 0.0, β = 1.0) μ = adj.	LC-BLYP (α = 0.2, β = 0.8) μ = adj.	LC-BLYP μ = 0.47	LC-BLYP (BS) μ = 0.47	CCSD(T)	CCSD(T)-F12
α (a.u.)								
1	140.14	140.14	139.14	139.50	131.73	131.73	123.33 (123.33)	123.92
2	323.26	323.26	327.87	327.03	290.62	290.62	267.20 (267.03)	272.71
3	558.04	558.04	584.22	577.84	483.61	483.61	439.70 (439.50)	454.19
4	825.12	825.12	893.36	875.60	695.05	695.05	627.67 (627.39)	654.38
5	1111.36	1111.36	1241.75	1206.20	916.30	916.30	824.27	865.75
6	1408.90	1408.90	1618.19	1558.40	1142.92	1142.92	1024.23	1081.85
MAE	176.64	176.64	249.69	229.70	58.97	58.97		
γ ($\times 10^3$ a.u.)								
1	116	116	115	112	93	93	110 (105)	104
2	964	964	982	951	666	666	522 (693)	624
3	3785	3785	4131	3952	2228	2228	2657 (2344)	2302
4	9670	9670	11,592	10,894	4949	4949	5366 (5146)	5231
5	18,913	18,913	25,091	23,088	8658	8658	8468	7909
6	31,133	31,133	45,508	40,903	13,086	13,086	13,866	11,220
MAE	5599	5599	9405	8152	330	330		

[a]All DFT and CCSD(T) calculations utilized the 6-31+G(d) basis with the CCSD(T)-F12 calculations using the cc-pVDZ basis and density-fitting approach described in the main text. The abbreviations "BS" and "μ = adj." indicate a broken-symmetry calculation and a nonempirically tuned value of μ, respectively. Values in parentheses denote the CCSD(T) values obtained by Champagne et al.[16]

Table 3. Longitudinal Linear Polarizability and Second Hyperpolarizability for Increasingly Large PBT Oligomers at Various Levels of Theory[a]

N	CAM-B3LYP	CAM-B3LYP (BS)	LC-BLYP (α = 0.0, β = 1.0) μ = adj.	LC-BLYP (α = 0.2, β = 0.8) μ = adj.	LC-BLYP μ = 0.47	LC-BLYP (BS) μ = 0.47	CCSD(T)	CCSD(T)-F12
α (a.u.)								
2	322.62	322.62	320.13	323.19	309.09	306.00	271.53 (271.51)	271.39
3	688.28	684.84	693.53	698.06	636.98	596.55	542.98 (542.83)	550.57
4	1196.72	1143.86	1235.13	1236.96	1069.64	955.85	894.94 (894.28)	918.93
5	1836.27	1693.92	1951.31	1942.37	1587.36	1363.60	1311.41	1364.21
6	2589.62	2315.23	2842.01	2811.11	2170.35	1804.02	1777.08	1870.96
MAE	367.11	272.51	448.83	442.75	195.10	45.62		
γ ($\times 10^3$ a.u.)								
2	363	363	403	374	341	552	543 (542)	303
3	2652	4387	2902	2698	2385	3469	3272 (3181)	1909
4	11,535	17,960	12,623	11,793	9361	11,804	10874 (11042)	9608
5	35,815	50,818	40,298	37,788	25,697	28,113	30,172	25,531
6	87,968	112,605	104,413	98,032	55,568	53,443	68,510	59,783
MAE	5312	14,624	9658	7760	4004	3652		

[a]All DFT and CCSD(T) calculations utilized the 6-31+G(d) basis with the CCSD(T)-F12 calculations using the cc-pVDZ basis and density-fitting approach described in the main text. The abbreviations "BS" and "μ = adj." indicate a broken-symmetry calculation and a nonempirically tuned value of μ, respectively. Values in parentheses denote the CCSD(T) values obtained by Champagne et al.[16]

the broken-symmetry solutions since the shaded regions (where a broken-symmetry solution is obtained) in Figure 2 lie to the right of the minima of all the J^2 curves. In other words, the ground-state wave function at the optimal μ values for PBT

DOI: 10.1021/acs.jctc.6b00360
J. Chem. Theory Comput. 2016, 12, 3593−3602

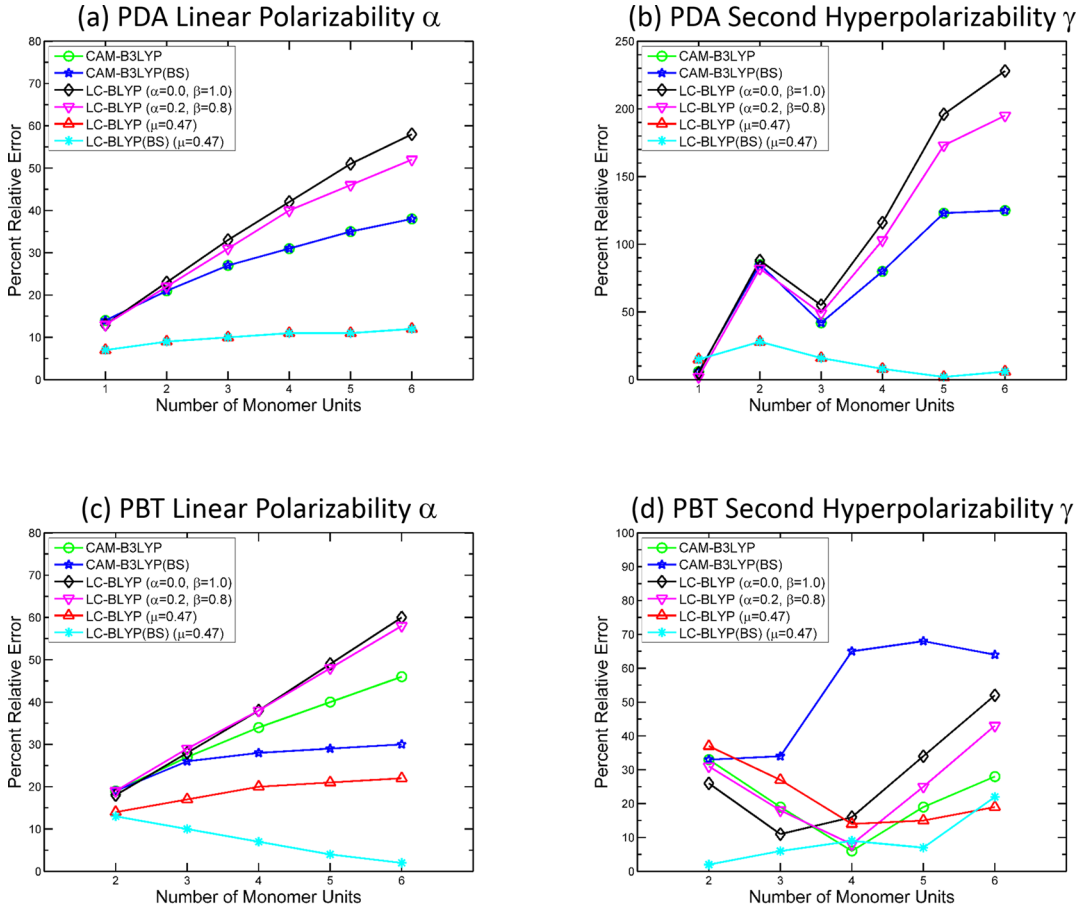

Figure 4. Percent relative error (compared to CCSD(T)) in α and γ as a function of number of monomer units in PDA (upper panel) and PBT (lower panel) for different levels of theory.

are closed-shell singlets and are not within the shaded regions in Figure 2. From these tabulated data entries, we observe an inverse correlation between the optimal μ values and the length of the oligomers, where μ decreases as the number of monomers increases. This general size-dependence in other chemical systems has been previously reported by several groups[20,49−52] and also in the previous study on PDA and PBT in ref 16. Our optimally tuned μ values are in excellent agreement with the LC-BLYP$_{\alpha=0.0,\beta=1.0}$ calculations given in the previous study by Champagne et al., shown in parentheses in Table 1. Specifically, we observe a negligible difference of ~0.005 Bohr^{-1}, and this deviation can be attributed to the difference between both tuning schemes. Reference 16 directly employs the DFT−Koopmans' theorem, where μ is tuned such that the energy of the −HOMO is equal to the IP, whereas we obtain μ by adjusting both the energy of the −HOMO to the IP and, in an indirect manner, the LUMO energy via the N + 1 electron system. All subsequent linear polarizability and second hyperpolarizability calculations were carried out using all of the optimal μ values listed in Table 1.

Tables 2 and 3 summarize the static longitudinal linear polarizability and second hyperpolarizability for the PDA and PBT oligomers, respectively, computed by the CAM-B3LYP, LC-BLYP$_{\alpha=0.0,\beta=1.0}$, LC-BLYP$_{\alpha=0.2,\beta=0.8}$, LC-BLYP(μ = 0.47), CCSD(T), and CCSD(T)-F12 methods. The broken-symmetry (BS) results for CAM-B3LYP and LC-BLYP(μ = 0.47) are also given in the tables for direct comparison to their closed-shell counterparts—recall that the optimally tuned LC-BLYP methods for both PDA and PBT were not affected by the broken-symmetry solutions. In addition, we also tabulated the $\langle S^2 \rangle$ values for both CAM-B3LYP (BS) and LC-BLYP (BS) (μ = 0.47) (cf. Table SI-12 in the Supporting Information) and found that while $\langle S^2 \rangle$ increases in size for PBT[2]−PBT[6], these systems are more accurately characterized as diradicals, without higher-lying spin states contributing to the trends in polarizability (cf. Figure SI-1, Tables SI-13, and SI-14 for LC-BLYP (BS) (μ = 0.47) calculations of the triplet state in the Supporting Information). All mean absolute errors (MAE) were computed with respect to the CCSD(T)/6-31+G(d) benchmarks to allow for a consistent comparison with the DFT calculations that were computed with the same 6-31+G(d) basis set. It is worth mentioning that the discrepancy between our results and previous CCSD(T) calculations of the hyperpolarizability[16] arise from the different numerical methodology and computational hardware used in these previous studies. Specifically, Champagne and co-workers utilized a Romberg differentiation procedure[53] for their calculations, whereas we directly fitted the CCSD(T) energies (as a function of the applied external field) to second- and fourth-order polynomials to obtain the linear polarizability and second hyperpolarizability, respectively. We found that the Romberg procedure was extremely sensitive to very small energy differences (even as small as 10^{-8} Hartrees), which can easily arise from different versions of software and machine architectures used in these previous studies. As such, all of the CCSD(T) results reported in this paper utilize the

DOI: 10.1021/acs.jctc.6b00360
J. Chem. Theory Comput. 2016, 12, 3593−3602

polynomial fitting procedure, which we found to be more numerically stable, for obtaining the linear polarizability and second hyperpolarizability. Furthermore, to check for possible nondynamical correlation effects in our CCSD(T) calculations, we also computed the T1 diagnostic for all of the oligomers and obtained T1 values ranging from 0.0125 to 0.0131 and 0.0156 to 0.0164 for PDA[1]−PDA[6] and PBT[2]−PBT[6], respectively (T1 values greater than 0.02 indicate that a multireference electron correlation method is necessary[54]). In addition, we also carried out broken-symmetry unrestricted CCSD(T) (UCCSD(T)) calculations for all of the PBT oligomers (cf. Figure SI-2 in the Supporting Information) and found that all of the UCCSD(T) energies using the broken-symmetry HF reference determinant were larger than their restricted CCSD(T) counterparts, further verifying (in conjunction with the T1 diagnostic discussed previously) that correlation effects are properly handled at the single-reference restricted CCSD(T) level of theory. Finally, we also did additional CCSD(T) calculations using the nondiffuse triple-ζ 6-311G(d,p) basis (cf. Table SI-15 in the Supporting Information) to assess the convergence of the 6-31+G(d,p) results used as benchmarks in both our study and the previous study by Champagne. We find that the presence of diffuse functions in the 6-31+G(d,p) basis plays a larger role than the additional valence basis functions in the 6-311G(d,p) basis, which is consistent with previous studies by Champagne and co-workers.[5,14] Furthermore, the explicitly correlated CCSD-(T)-F12 calculations closely mirror the overall trends in the CCSD(T)/6-31+G(d) methods, giving additional indication of the basis-set convergence of our calculations.

Figure 4 presents a graphical summary of Tables 2 and 3 by plotting the percent relative error for each of the various DFT methods using the CCSD(T)/6-31+G(d) calculations as benchmarks. Our calculations of the PDA linear polarizabilities (α) in Figure 4(a) using CAM-B3LYP, LC-BLYP(μ = 0.47) and CCSD(T) are in accordance with the values computed in ref 16. As mentioned in the Introduction, the previous work by Champagne and co-workers did not compute the CCSD(T) polarizabilities for the largest PDA and PBT chains with five and six oligomers, and therefore, the overall trends in their range-separated calculations could not be checked to see if the extrapolated DFT trends would either degrade or improve as a function of oligomer size. By completing these computationally expensive benchmarks, we can now state that the same dramatic overestimation of the longitudinal linear polarizability with the nonempirically tuned LC-BLYP$_{\alpha=0.0,\beta=1.0}$ functional persists for large oligomers. However, in contrast to previous findings,[16] we find that the accuracy of the linear polarizability does improve when a small amount of HF exchange is included at short-range (LC-BLYP$_{\alpha=0.2,\beta=0.8}$) compared to the "base" LC-BLYP$_{\alpha=0.0,\beta=1.0}$ approach (a reduction in the MAE from 249.69 to 229.70 au is observed). Moreover, the accuracy of LC-BLYP$_{\alpha=0.2,\beta=0.8}$ appears to further improve as a function of the number monomer units, N, particularly for $N \geq 3$. The CAM-B3LYP functional gives more accurate predictions of the linear polarizability than either of the nonempirically tuned LC-BLYP methods, but the LC-BLYP(μ = 0.47) functional gives the best agreement (with the lowest MAE values of 58.97 au) compared to CCSD(T) benchmarks, which is consistent with ref 16 and previous work on polarizabilities by other groups.[39] Turning to the second hyperpolarizabilities (γ) of PDA, Figure 4(b) shows a similar trend in accuracy compared to Figure 4(a) for the linear polarizabilities. As before, incorporating some portion of short-range HF exchange does improve the overall accuracy as a function of oligomer size; however, the most accurate second hyperpolarizabilities are still obtained with the LC-BLYP(μ = 0.47) functional (MAE = 330 au). Moreover, as shown in Figures 4(a) and (b), there is no change in either α or γ when the stability of the wave function is taken into consideration since the ground states of all the PDA oligomers have a closed-shell solution regardless of μ value.

Turning to the PBT oligomers, we find that the overestimation of the static linear polarizability (α) is more severe than for PDA. Similar to Figure 4(a), we also find that the polarizabilities are improved by including some short-range HF exchange, although the difference between these methods is smaller in the PBT system (MAEs for LC-BLYP$_{\alpha=0.0,\beta=1.0}$ vs LC-BLYP$_{\alpha=0.0,\beta=1.0}$ in PBT are 448.83 and 442.75 au, respectively). However, in contrast to the PDA chains, the PBT oligomers are much more strongly conjugated along their backbone and can converge toward a lower-energy broken-symmetry solution. As mentioned previously, DFT methods that contain a large percentage of HF exchange will favor an unrestricted open-shell configuration, and we find that a lower-energy broken-symmetry solution is actually *preferred* in CAM-B3LYP and LC-BLYP(μ = 0.47) for PBT. Interestingly, as the amount of HF exchange is increased in the XC-functional, the slope in the error of the static linear polarizability (as a function of oligomer size) decreases, as shown in Figure 4(c). However, it is worth noting that increasing the amount of HF exchange to 100% (i.e., pure Hartree−Fock) will lead to severe overestimations for both α and γ as a function of size (cf. Figure SI-2 and Tables SI-13 and SI-14 in the Supporting Information). In the case of PBT, the characteristic plateau in the asymptotic limit, which still corresponds to a fairly large ∼20% percent error, is reached for LC-BLYP(μ = 0.47). However, for the PBT linear polarizabilities, the broken-symmetry solutions give a more accurate result compared to their restricted, closed-shell counterparts in all cases. Specifically, allowing the system to relax to a lower-energy broken-symmetry solution with CAM-B3LYP leads to a constant value for the linear polarizability as N increases, where the associated error is less than 30%. This is in stark contrast to the *growing* error of ∼45% in the restricted, closed-shell CAM-B3LYP method. A remarkably different behavior is obtained with the broken-symmetry LC-BLYP(μ = 0.47) method where a negative slope as a function of oligomer size is obtained, resulting in a relative error of less than 5% when $N > 4$. As mentioned previously, we also carried out LC- BLYP (BS) (μ = 0.47) calculations of the triplet state (cf. Figure SI-1 in the Supporting Information) and found that the errors in the linear polarizability were larger than their LC-BLYP (BS) singlet state counterparts, further confirming that these systems are more accurately characterized as diradicals, without higher-lying spin states contributing to the trends in polarizability. In summary, the MAEs for the linear polarizabilities in PBT can be summarized as follows: α[LC-BLYP(μ = 0.47) (BS)] ≪ α[LC-BLYP(μ = 0.47)] < α[CAM-B3LYP (BS)] < α[CAM-B3LYP] < α[LC-BLYP$_{\alpha=0.2,\beta=0.8}$ (μ adj.)] < α[LC-BLYP$_{\alpha=0.0,\beta=1.0}$ (μ adj.)]. Finally, we now turn to the second hyperpolarizabilities of PBT, whose relative errors are smaller in comparison to the values obtained for PDA. From Figure 4(d), we observe that a poor accuracy is obtained in the hyperpolarizability values when a broken-symmetry CAM-B3LYP approach is applied. However, similar to our findings with the linear polarizabilities in PDA, the use of LC-BLYP(μ = 0.47) with the lower-energy broken-symmetry solution

DOI: 10.1021/acs.jctc.6b00360
J. Chem. Theory Comput. 2016, 12, 3593−3602

improves the accuracy of the second hyperpolarizability. As such, the MAEs for the second hyperpolarizabilites in PBT can be summarized as follows: γ[LC-BLYP(μ = 0.47) (BS)] < γ[LC-BLYP(μ = 0.47)] < γ[CAM-B3LYP] < γ[LC-BLYP$_{\alpha=0.2,\beta=0.8}$ (μ adj.)] < γ[LC-BLYP$_{\alpha=0.0,\beta=1.0}$ (μ adj.)] < γ[CAM-B3LYP (BS)]. Among all the DFT methods examined here, the broken-symmetry LC-BLYP(μ = 0.47) functional is the most accurate for *both* α and γ in PBT, highlighting the importance of broken-symmetry effects when calculating polarizabilities and hyperpolarizabilties of these π-conjugated oligomers.

CONCLUSIONS

In this study, we have calculated and analyzed the static linear polarizability and second-order hyperpolarizabilities for several PDA and PBT oligomers using a variety of range-separated DFT methods. Specifically, we have examined a diverse set of nonempirically tuned range-separated functionals with both short- and long-range exchange as well as conventional CAM-B3LYP and LC-BLYP range-separated hybrids with fixed values of μ (namely, LC-BLYP(μ = 0.47)). To test the accuracy of these various range-separated methods, we calculated new large-scale CCSD(T) and explicitly correlated CCSD(T)-F12 benchmarks for the PDA and PBT systems, which extends previous benchmarks on these systems that were limited to smaller oligomers. Most importantly, these new CCSD(T) and CCSD(T)-F12 calculations comprise the most complete and accurate calculations of linear polarizabilities and second hyperpolarizabilites on these systems to date.

Contrary to previous studies on these systems, we find that the inclusion of some amount of short-range exchange *does* improve the accuracy of the computed polarizabilities for both PDA and PBT, although the degree of improvement is more modest for the linear polarizability compared to the second hyperpolarizability. More importantly, in contrast to prior studies on these same systems, we find that the lowest-energy electronic states for PBT are *not* closed-shell singlets, and improved accuracy with range-separated functionals can be obtained by allowing the system to relax to a lower-energy broken-symmetry solution. This enhanced accuracy is most pronounced in the broken-symmetry LC-BLYP(μ = 0.47) functional, which attains a relative error of less than 10% for the linear polarizability. Similarly, the computed second hyperpolarizabilities are also significantly improved by allowing for a lower-energy broken-symmetry solution in the LC-BLYP(μ = 0.47) calculations. Recent studies on molecular polarizabilities have advocated for the use of range-separated methods with large μ values (which correspond to larger amounts of HF exchange), and it is well known that DFT methods containing a large contribution of HF exchange will naturally favor an unrestricted open-shell configuration. We now expand these statements to add that one should carefully check for a broken-symmetry solution when computing linear polarizabilities and second hyperpolarizabilites with range-separated functionals, particularly for π-conjugated systems. To the best of our knowledge, this present study is the first to highlight the improved accuracy of range-separated methods for polarizabilities and second hyperpolarizabilites when a lower-energy broken-symmetry solution is obtained. On a practical note, since many novel NLO polymer materials are strongly conjugated, it is crucial to test for a lower-energy open-shell configuration in their ground state when calculating NLO properties with range-separated functionals. Taken together, these new broken-symmetry range-separated DFT calculations in conjunction with our high-level CCSD(T) and CCSD(T)-F12 benchmarks emphasize and highlight the importance of broken-symmetry effects when calculating linear polarizabilities and second hyperpolarizabilties of π-conjugated chains.

ASSOCIATED CONTENT

Supporting Information

The Supporting Information is available free of charge on the ACS Publications website at DOI: 10.1021/acs.jctc.6b00360.

Reference Cartesian coordinates for all the PDA and PBT oligomers utilized in this study, $\langle S^2 \rangle$ values for the CAM-B3LYP (BS) and LC-BLYP (BS) (μ = 0.47) functionals, relative error in α for PBT at the LC-BLYP (BS) (μ = 0.47) level of theory for the triplet state, longitudinal linear polarizability and second hyperpolarizability for PDA and PBT oligomers at the triplet LC-BLYP (BS) (μ = 0.47) and HF (BS) levels of theory, energy difference between broken-symmetry unrestricted CCSD(T) (BS-UCCSD(T)) and restricted CCSD(T) for PBT, longitudinal linear polarizability and second hyperpolarizability for PDA and PBT oligomers at the CCSD(T)/6-311G(d,p) level of theory, and relative error in α and γ for PDA and PBT at the Hartree−Fock level of theory.(PDF)

AUTHOR INFORMATION

Corresponding Author

*E-mail: bryan.wong@ucr.edu. Homepage: http://www.bmwong-group.com.

Notes

The authors declare no competing financial interest.

ACKNOWLEDGMENTS

We gratefully acknowledge Prof. Benoît Champagne for providing the Cartesian coordinates for all of the PDA and PBT oligomers used in this work. Support from the National Science Foundation, Institute for Complex Adaptive Matter (NSF-ICAM), is acknowledged. We acknowledge the National Science Foundation for the use of supercomputing resources through the Extreme Science and Engineering Discovery Environment (XSEDE), Project No. TG- DMR140054.

REFERENCES

(1) Franken, P. A.; Hill, A. E.; Peters, C. W.; Weinreich, G. Generation of Optical Harmonics. *Phys. Rev. Lett.* **1961**, *7*, 118−119.
(2) Armstrong, J. A.; Bloembergen, N.; Ducuing, J.; Pershan, P. S. Interactions Between Light Waves in a Nonlinear Dielectric. *Phys. Rev.* **1962**, *127*, 1918−1939.
(3) Bloembergen, N.; Pershan, P. S. Light Waves at the Boundary of Nonlinear Media. *Phys. Rev.* **1962**, *128*, 606−622.
(4) Champagne, B.; Bishop, D. Calculations of Nonlinear Optical Properties for the Solid State. *Adv. Chem. Phys.* **2003**, *126*, 41−92.
(5) Champagne, B.; Bulat, F. A.; Yang, W. T.; Bonness, S.; Kirtman, B. Density Functional Theory Investigation of the Polarizability and Second Hyperpolarizability of Polydiacetylene and Polybutatriene Chains: Treatment of Exact Exchange and Role of Correlation. *J. Chem. Phys.* **2006**, *125*, 194114.
(6) Dalton, L. Nonlinear Optical Polymeric Materials: From Chromophore Design to Commercial Applications. *Polym. Photon. Applicat. I* **2002**, *158*, 1−86.

(7) Schindler, F.; Lupton, J. M.; Muller, J.; Feldmann, J.; Scherf, U. How Single Conjugated Polymer Molecules Respond to Electric Fields. *Nat. Mater.* **2006**, *5*, 141−146.
(8) Kurtz, H. A.; Dudis, D. S. Quantum Mechanical Methods for Predicting Nonlinear Optical Properties. *Rev. Comput. Chem.* **1998**, *12*, 241−280.
(9) Jacquemin, D.; Perpète, E. A.; Scalmani, G.; Frisch, M. J.; Kobayashi, R.; Adamo, C. Assessment of the Efficiency of Long-Range Corrected Functionals for Some Properties of Large Compounds. *J. Chem. Phys.* **2007**, *126*, 144105.
(10) Jacquemin, D.; Perpète, E. A.; Scalmani, G.; Frisch, M. J.; Kobayashi, R.; Adamo, C.; Medved, M. First Hyperpolarizability of Polymethineimine with Long-Range Corrected Functionals. *J. Chem. Phys.* **2007**, *126*, 191108.
(11) Li, Q. X.; Chen, L. P.; Li, Q. K.; Shuai, Z. G. Electron Correlation Effects on the Nonlinear Optical Properties of Conjugated Polyenes. *Chem. Phys. Lett.* **2008**, *457*, 276−278.
(12) Cohen, A. J.; Mori-Sánchez, P.; Yang, W. Challenges for Density Functional Theory. *Chem. Rev.* **2012**, *112*, 289−320.
(13) Champagne, B.; Perpète, E. A.; Jacquemin, D.; van Gisbergen, S. J.; Baerends, E.-J.; Soubra-Ghaoui, C.; Robins, K. A.; Kirtman, B. Assessment of Conventional Density Functional Schemes for Computing the Dipole Moment and (Hyper) Polarizabilities of Push-Pull π-Conjugated Systems. *J. Phys. Chem. A* **2000**, *104*, 4755−4763.
(14) Champagne, B.; Perpete, E. A.; van Gisbergen, S. J. A.; Baerends, E. J.; Snijders, J. G.; Soubra-Ghaoui, C.; Robins, K. A.; Kirtman, B. Assessment of Conventional Density Functional Schemes for Computing the Polarizabilities and Hyperpolarizabilities of Conjugated Oligomers: An Ab Initio Investigation of Polyacetylene Chains. *J. Chem. Phys.* **1998**, *109*, 10489−10498.
(15) Champagne, B.; Perpete, E. A. Bond Length Alternation Effects on the Static Electronic Polarizability and Second Hyperpolarizability of Polyacetylene Chains. *Int. J. Quantum Chem.* **1999**, *75*, 441−447.
(16) Nenon, S.; Champagne, B.; Spassova, M. I. Assessing Long-Range Corrected Functionals with Physically-Adjusted Range-Separated Parameters for Calculating the Polarizability and the Second Hyperpolarizability of Polydiacetylene and Polybutatriene Chains. *Phys. Chem. Chem. Phys.* **2014**, *16*, 7083−7088.
(17) Raeber, A. E.; Wong, B. M. The Importance of Short- and Long-Range Exchange on Various Excited State Properties of DNA Monomers, Stacked Complexes, and Watson-Crick Pairs. *J. Chem. Theory Comput.* **2015**, *11*, 2199−2209.
(18) Egger, D. A.; Weissman, S.; Refaely-Abramson, S.; Sharifzadeh, S.; Dauth, M.; Baer, R.; Kummel, S.; Neaton, J. B.; Zojer, E.; Kronik, L. Outer-valence Electron Spectra of Prototypical Aromatic Heterocycles from an Optimally Tuned Range-Separated Hybrid Functional. *J. Chem. Theory Comput.* **2014**, *10*, 1934−1952.
(19) Refaely-Abramson, S.; Sharifzadeh, S.; Govind, N.; Autschbach, J.; Neaton, J. B.; Baer, R.; Kronik, L. Quasiparticle Spectra from a Nonempirical Optimally Tuned Range-Separated Hybrid Density Functional. *Phys. Rev. Lett.* **2012**, *109*, 226405.
(20) Rohrdanz, M. A.; Martins, K. M.; Herbert, J. M. A Long-Range-Corrected Density Functional that Performs Well for Both Ground-State Properties and Time-Dependent Density Functional Theory Excitation Energies, Including Charge-Transfer Excited States. *J. Chem. Phys.* **2009**, *130*, 054112.
(21) Srebro, M.; Autschbach, J. Does a Molecule-Specific Density Functional Give an Accurate Electron Density? The Challenging Case of the CuCl Electric Field Gradient. *J. Phys. Chem. Lett.* **2012**, *3*, 576−581.
(22) Paldus, J.; Čížek, J. Hartree−Fock Stability and Symmetry Breaking: Oxygen Doubly Negative Ion. *Can. J. Chem.* **1985**, *63*, 1803−1811.
(23) Sherrill, C. D.; Lee, M. S.; Head-Gordon, M. On the Performance of Density Functional Theory for Symmetry-Breaking Problems. *Chem. Phys. Lett.* **1999**, *302*, 425−430.
(24) Tawada, Y.; Tsuneda, T.; Yanagisawa, S.; Yanai, T.; Hirao, K. A Long-Range-Corrected Time-Dependent Density Functional Theory. *J. Chem. Phys.* **2004**, *120*, 8425−8433.
(25) Toulouse, J.; Colonna, F.; Savin, A. Long-Range−Short-Range Separation of the Electron-Electron Interaction in Density-Functional Theory. *Phys. Rev. A: At., Mol., Opt. Phys.* **2004**, *70*, 062505.
(26) Tawada, Y.; Tsuneda, T.; Yanagisawa, S.; Yanai, T.; Hirao, K. A Long-Range-Corrected Time-Dependent Density Functional Theory. *J. Chem. Phys.* **2004**, *120*, 8425−8433.
(27) Toulouse, J.; Colonna, F.; Savin, A. Long-Range-Short-Range Separation of the Electron-Electron Interaction in Density-Functional Theory. *Phys. Rev. A: At., Mol., Opt. Phys.* **2004**, *70*, 062505.
(28) Yanai, T.; Tew, D. P.; Handy, N. C. A New Hybrid Exchange−Correlation Functional Using the Coulomb-Attenuating Method (CAM-B3LYP). *Chem. Phys. Lett.* **2004**, *393*, 51−57.
(29) Wong, B. M.; Cordaro, J. G. Coumarin Dyes for Dye-Sensitized Solar Cells: A Long-Range-Corrected Density Functional Study. *J. Chem. Phys.* **2008**, *129*, 214703.
(30) Foster, M. E.; Wong, B. M. Nonempirically Tuned Range-Separated DFT Accurately Predicts Both Fundamental and Excitation Gaps in DNA and RNA Nucleobases. *J. Chem. Theory Comput.* **2012**, *8*, 2682−2687.
(31) Wong, B. M.; Hsieh, T. H. Optoelectronic and Excitonic Properties of Oligoacenes: Substantial Improvements from Range-Separated Time-Dependent Density Functional Theory. *J. Chem. Theory Comput.* **2010**, *6*, 3704−3712.
(32) Foster, M. E.; Azoulay, J. D.; Wong, B. M.; Allendorf, M. D. Novel Metal-Organic Framework Linkers for Light Harvesting Applications. *Chem. Sci.* **2014**, *5*, 2081−2090.
(33) Wong, B. M.; Piacenza, M.; Sala, F. D. Absorption and Fluorescence Properties of Oligothiophene Biomarkers from Long-Range-Corrected Time-Dependent Density Functional Theory. *Phys. Chem. Chem. Phys.* **2009**, *11*, 4498−4508.
(34) Richard, R. M.; Herbert, J. M. Time-Dependent Density-Functional Description of the 1La State in Polycyclic Aromatic Hydrocarbons: Charge-Transfer Character in Disguise? *J. Chem. Theory Comput.* **2011**, *7*, 1296−1306.
(35) Kuritz, N.; Stein, T.; Baer, R.; Kronik, L. Charge-Transfer-Like $\pi \rightarrow \pi^*$ Excitations in Time-Dependent Density Functional Theory: A Conundrum and Its Solution. *J. Chem. Theory Comput.* **2011**, *7*, 2408−2415.
(36) Stein, T.; Kronik, L.; Baer, R. Prediction of Charge-Transfer Excitations in Coumarin-Based Dyes Using a Range-Separated Functional Tuned from First Principles. *J. Chem. Phys.* **2009**, *131*, 244119.
(37) Kronik, L.; Stein, T.; Refaely-Abramson, S.; Baer, R. Excitation Gaps of Finite-Sized Systems from Optimally Tuned Range-Separated Hybrid Functionals. *J. Chem. Theory Comput.* **2012**, *8*, 1515−1531.
(38) Stein, T.; Kronik, L.; Baer, R. Reliable Prediction of Charge Transfer Excitations in Molecular Complexes Using Time-Dependent Density Functional Theory. *J. Am. Chem. Soc.* **2009**, *131*, 2818−2820.
(39) Garrett, K.; Sosa Vazquez, X. A.; Egri, S. B.; Wilmer, J.; Johnson, L. E.; Robinson, B. H.; Isborn, C. M. Optimum Exchange for Calculation of Excitation Energies and Hyperpolarizabilities of Organic Electro-optic Chromophores. *J. Chem. Theory Comput.* **2014**, *10*, 3821−3831.
(40) Frisch, M. J.; Trucks, G. W.; Schlegel, H. B.; Scuseria, G. E.; Robb, M. A.; Cheeseman, J. R.; Scalmani, G.; Barone, V.; Mennucci, B.; Petersson, G. A.; Nakatsuji, H.; Caricato, M.; Li, X.; Hratchian, H. P.; Izmaylov, A. F.; Bloino, J.; Zheng, G.; Sonnenberg, J. L.; Hada, M.; Ehara, M.; Toyota, K.; Fukuda, R.; Hasegawa, J.; Ishida, M.; Nakajima, T.; Honda, Y.; Kitao, O.; Nakai, H.; Vreven, T.; Montgomery, Jr., J. A.; Peralta, J. E.; Ogliaro, F.; Bearpark, M. J.; Heyd, J.; Brothers, E. N.; Kudin, K. N.; Staroverov, V. N.; Kobayashi, R.; Normand, J.; Raghavachari, K.; Rendell, A. P.; Burant, J. C.; Iyengar, S. S.; Tomasi, J.; Cossi, M.; Rega, N.; Millam, N. J.; Klene, M.; Knox, J. E.; Cross, J. B.; Bakken, V.; Adamo, C.; Jaramillo, J.; Gomperts, R.; Stratmann, R. E.; Yazyev, O.; Austin, A. J.; Cammi, R.; Pomelli, C.; Ochterski, J. W.; Martin, R. L.; Morokuma, K.; Zakrzewski, V. G.;

DOI: 10.1021/acs.jctc.6b00360
J. Chem. Theory Comput. 2016, 12, 3593−3602

Voth, G. A.; Salvador, P.; Dannenberg, J. J.; Dapprich, S.; Daniels, A. D.; Farkas, Ö.; Foresman, J. B.; Ortiz, J. V.; Cioslowski, J.; Fox, D. J. *Gaussian 09*, Gaussian, Inc.: Wallingford, CT, USA, 2009.
(41) Tew, D. P.; Klopper, W.; Neiss, C.; Hattig, C. Quintuple-[small zeta] Quality Coupled-Cluster Correlation Energies with Triple-[small zeta] Basis Sets. *Phys. Chem. Chem. Phys.* **2007**, *9*, 1921−1930.
(42) Knizia, G.; Adler, T. B.; Werner, H.-J. Simplified CCSD(T)-F12 Methods: Theory and Benchmarks. *J. Chem. Phys.* **2009**, *130*, 054104.
(43) Adler, T. B.; Knizia, G.; Werner, H.-J. A simple and Efficient CCSD(T)-F12 Approximation. *J. Chem. Phys.* **2007**, *127*, 221106.
(44) Jimenez-Hoyos, C. A.; Rodriguez-Guzman, R.; Scuseria, G. E. Polyradical Character and Spin Frustration in Fullerene Molecules: An Ab Initio Non-Collinear Hartree-Fock Study. *J. Phys. Chem. A* **2014**, *118*, 9925−9940.
(45) Masunov, A. E.; Anderson, D.; Freidzon, A. Y.; Bagaturyants, A. A. Symmetry-Breaking in Cationic Polymethine Dyes: Part 2. Shape of Electronic Absorption Bands Explained by the Thermal Fluctuations of the Solvent Reaction Field. *J. Phys. Chem. A* **2015**, *119*, 6807−6815.
(46) Sherrill, C. D.; Lee, M. S.; Head-Gordon, M. On the Performance of Density Functional Theory for Symmetry-Breaking Problems. *Chem. Phys. Lett.* **1999**, *302*, 425−430.
(47) Thompson, L. M.; Hratchian, H. P. Modeling the Photoelectron Spectra of MoNbO2- Accounting for Spin Contamination in Density Functional Theory. *J. Phys. Chem. A* **2015**, *119*, 8744−8751.
(48) Yesudas, K. Cationic Cyanine Dyes: Impact of Symmetry-Breaking on Optical Absorption and Third-Order Polarizabilities. *Phys. Chem. Chem. Phys.* **2013**, *15*, 19465−19477.
(49) Wong, B. M.; Hsieh, T. H. Optoelectronic and Excitonic Properties of Oligoacenes: Substantial Improvements from Range-Separated Time-Dependent Density Functional Theory. *J. Chem. Theory Comput.* **2010**, *6*, 3704−3712.
(50) Wong, B. M.; Cordaro, J. G. Coumarin Dyes for Dye-Sensitized Solar Cells: A Long-Range-Corrected Density Functional Study. *J. Chem. Phys.* **2008**, *129*, 214703.
(51) Rohrdanz, M. A.; Herbert, J. M. Simultaneous Benchmarking of Ground- and Excited-State Properties with Long-Range-Corrected Density Functional Theory. *J. Chem. Phys.* **2008**, *129*, 034107.
(52) Stein, T.; Kronik, L.; Baer, R. Prediction of Charge-Transfer Excitations in Coumarin-Based Dyes Using a Range-Separated Functional Tuned from First Principles. *J. Chem. Phys.* **2009**, *131*, 244119.
(53) Medveď, M.; Stachová, M.; Jacquemin, D.; André, J.-M.; Perpète, E. A. A Generalized Romberg Differentiation Procedure for Calculation of Hyperpolarizabilities. *J. Mol. Struct.: THEOCHEM* **2007**, *847*, 39−46.
(54) Lee, T. J.; Taylor, P. R. A Diagnostic for Determining the Quality of Single-Reference Electron Correlation Methods. *Int. J. Quantum Chem.* **1989**, *36*, 199−207.

DOI: 10.1021/acs.jctc.6b00360
J. Chem. Theory Comput. 2016, 12, 3593−3602